

Spin-strain interactions under hydrostatic pressure in α -RuCl₃

A. Hauspurg,^{1,2} Susmita Singh,³ T. Yanagisawa,⁴ V. Tsurkan,^{5,6} J. Wosnitzer,^{1,2} Wolfram Brenig,⁷ Natalia B. Perkins,^{3,8} and S. Zherlitsyn¹

¹*Hochfeld-Magnetlabor Dresden (HLD-EMFL) and Würzburg-Dresden Cluster of Excellence ct.qmat, Helmholtz-Zentrum Dresden-Rossendorf (HZDR), 01328 Dresden, Germany*

²*Institut für Festkörper- und Materialphysik, TU Dresden, 01062 Dresden, Germany*

³*School of Physics and Astronomy, University of Minnesota, Minneapolis, Minnesota 55455, USA*

⁴*Department of Physics, Hokkaido University, Sapporo 060-0810, Japan*

⁵*Experimental Physics V, Center for Electronic Correlations and Magnetism, University of Augsburg, 86135 Augsburg, Germany*

⁶*Institute of Applied Physics, Moldova State University, MD 2028, Chisinau, Republic of Moldova*

⁷*Institute for Theoretical Physics, Technical University Braunschweig, 38106 Braunschweig, Germany*

⁸*Technical University of Munich, Germany, Institute for Advanced Study, 85748 Garching, Germany*

(Dated: March 7, 2025)

We investigate the effects of hydrostatic pressure on α -RuCl₃, a prototypical material for the Kitaev spin model on a honeycomb lattice with a possible spin-liquid ground state. Using ultrasound measurements at pressures up to 1.16 GPa, we reveal significant modifications of the acoustic properties and the H - T phase diagram of this material. Hydrostatic pressure suppresses the three-dimensional magnetic order and induces a dimerization transition at higher pressures. At low pressures, the sound attenuation exhibits a linear temperature dependence, while above 0.28 GPa, it becomes nearly temperature independent, suggesting a shift in the phonon scattering regime dominated by Majorana fermions. These findings provide new insights into spin-strain interactions in Kitaev magnets and deliver a detailed characterization of the H - T phase diagram of α -RuCl₃ under hydrostatic pressure.

I. INTRODUCTION

In recent years, significant efforts have been focused on finding materials with bond-dependent Ising-like interactions that could realize the spin-1/2 Kitaev honeycomb model [1–4] and its quantum spin-liquid (QSL) state with fractionalized excitations – Majorana fermions and Z_2 fluxes [5]. Although, so far, no material has been confirmed as a perfect realization of this idealized model, the $J_{\text{eff}} = 1/2$ strongly spin-orbit-coupled Mott insulator α -RuCl₃ [6–14] stands out as a promising candidate to investigate the intriguing physics of Kitaev quantum spin liquids. Despite exhibiting a zigzag antiferromagnetic (AFM) order below 7 K, indicating deviations from the pure Kitaev model due to subdominant non-Kitaev interactions, various dynamical probes suggest that α -RuCl₃ lies in close proximity to a QSL state [8–10, 15, 16]. Among the many dynamical probes proposed to study this proximity [17–30], recent studies have identified phonon dynamics as a particularly promising and insightful tool. This approach is particularly relevant for α -RuCl₃, where spin-lattice coupling plays a crucial role in its various properties and phenomena [8, 31–42].

Ultrasound measurements of sound velocity and attenuation provide an effective method for investigating the dynamics of acoustic phonons [43, 44], a technique recently applied to α -RuCl₃ to explore its temperature and magnetic-field dependences of sound attenuation [45]. This study revealed that the dominant processes contributing to the sound attenuation in this material can be attributed to phonons scattering off fractionalized excitations, thus supporting the idea of proximity of α -RuCl₃ to the Kitaev QSL [33, 34, 46–49].

Lattice degrees of freedom have not only been of interest in the context of dynamical phonons coupled to a proximate

QSL, but also significant attention has been devoted to studying the effects of hydrostatic pressure on α -RuCl₃. In this work, we, therefore, make the natural step forward to combine the static and dynamic aspects of the coupling between the lattice, the magnetic, and electronic degrees of freedom in α -RuCl₃, by investigating ultrasound propagation under hydrostatic pressure. This offers valuable insights into the nature of the magnetic state and the interplay between spin and lattice degrees of freedom.

A prime ingredient of our study is that α -RuCl₃ under hydrostatic pressure undergoes a dimerization and a suppression of the magnetic ground state above a critical pressure P_c . To apply hydrostatic pressure, different experimental approaches have been utilized. The first involves the use of piston-type pressure cells, combined with pressure media such as Daphne 7373 [50–52]. This is also employed in the present study. The second approach employs He-gas pressure cells [52–55]. These cells offer the advantage of in situ pressure adjustment at low temperatures, provided the temperature remains above the crystallization point of ⁴He [56]. The third approach by Wang *et al.* in [57] resorts to a toroid-type pressure cell with a glycerin/water mixture as the pressure medium, as well as a diamond anvil cell using NaCl as the pressure medium.

Remarkably, and while all methods agree on the existence of a critical pressure P_c , its reported value varies among the techniques. Using ⁴He as pressure medium, P_c is 0.1–0.2 GPa [50–52, 55], whereas using Daphne 7373, P_c is 0.7–1 GPa [52–54]. A key observation is that pressure affects both spin and structural properties in a non-monotonic manner. Even before lattice dimerization, pressure partly suppresses magnetic ordering, evident as a gradual reduction in the Néel temperature, T_N , up to 0.25 GPa in piston-cell experiments [53, 54]. Beyond 0.25 GPa, T_N increases, leading to com-

plete suppression of magnetic ordering at P_c .

To further explore the influence of such hydrostatic pressure on Kitaev physics and magnetoelastic coupling, we present a study employing ultrasound techniques, which are highly sensitive to phase transitions [43–45], and examine how spin-strain interactions evolve under varying pressure. We observe that applied pressure increases the velocity of the transverse acoustic mode $(c_{11} - c_{12})/2$. However, this change is nonlinear with pressure. Additionally, the attenuation of this mode changes from a linear temperature dependence to being nearly temperature independent.

To interpret these findings, we performed theoretical estimates of the sound attenuation. Our study reveals that the temperature dependence of the sound attenuation in α - RuCl_3 is consistent with scattering of phonons by fractionalized excitations, a hallmark of the material’s proximity to a Kitaev QSL. Our results also show that pressure-induced variations in the sound velocity and coupling constants are key to understanding the change of the sound attenuation versus pressure. Namely, within the pure Kitaev model, increasing pressure reduces the magnitude of the Kitaev coupling K [54]. As our experiment shows an increase in sound velocity, this leads to a critical pressure, at which the sound velocity surpasses the Fermi velocity. This, in turn, causes the dominant scattering mechanism to shift from particle-hole to particle-particle processes, resulting in a transition from a linear increase of the sound attenuation with temperature, via an almost temperature-independent behavior, to a decrease with temperature [33, 34]. Expanding our analysis to the J - K - Γ model reveals similar trends, though the transition occurs at slightly higher pressures. This shift is attributed to the growing influence of Heisenberg J and off-diagonal Γ interactions, which further modify the Majorana fermion spectrum in α - RuCl_3 .

We also investigated the pressure dependence of the H - T phase diagram for α - RuCl_3 with an in-plane magnetic field ($H \parallel a$), extending our measurements to hydrostatic pressures as high as 1.16 GPa. This approach provides valuable insights into the intricate coupling mechanisms and pressure-induced modifications of the magnetic and structural properties of this material.

II. EXPERIMENTAL DETAILS

A. Sample preparation and characterization

We grew high-quality single crystals of α - RuCl_3 by vacuum sublimation [14, 59]. The samples show a single ordering temperature of approximately 7 K [Fig. 2(a)] and no signature of any additional phase transition at 14 K, typically caused by stacking faults [60]. At room temperature, α - RuCl_3 has a trigonal structure with $P3_112$ space group [15, 61]. Upon cooling, the material undergoes a first-order structural transition at about 140 K accompanied by a large hysteresis, though the precise low-temperature structure remains under debate [62, 63]. Weak van der Waals interactions between the layers may result in different stacking orders of the honey-

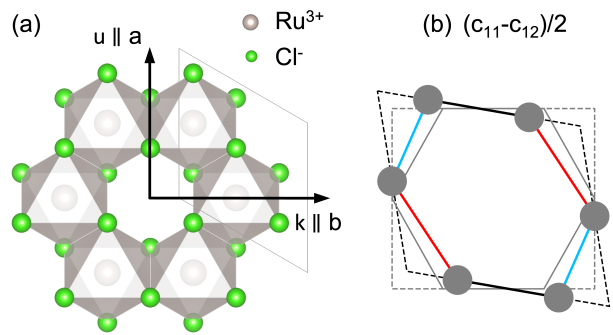


FIG. 1. (a) Crystal structure of α - RuCl_3 in a honeycomb plane and the crystallographic directions with the notations used in this work. Green and gray spheres indicate the positions of Cl^- and Ru^{3+} ions, respectively. The sound-propagation direction k and polarization u for the transverse acoustic mode $(c_{11} - c_{12})/2$ are shown. The thin lines represent the primitive unit cell in the ab plane. Crystal structure created using Vesta [58]. (b) Lattice strain (bold lines) related to the transverse acoustic mode $(c_{11} - c_{12})/2$ for a hexagonal lattice. Dashed lines represent the local symmetry before and after the deformation.

comb planes, with minimal energy differences between stacking configurations [61, 64].

The samples are oriented using Laue x-ray backscattering diffraction. For clarity, we distinguish between the crystallographic directions within the honeycomb plane: The direction perpendicular to the Ru-Ru bonds (equivalent to a) and the direction parallel to the Ru-Ru bonds (equivalent to b), as illustrated in Fig. 1(a). For the ultrasound experiments the surfaces of the samples are treated with a focused ion beam (FIB) [45]. This technique proves to process the sample surfaces with low mechanical wear, such that the fragile stacking order of the honeycomb planes is not disturbed. The sample dimensions are 1.63 mm along the sound propagation direction b , and approximately 0.5 mm along the c -axis, perpendicular to the honeycomb plane.

B. Ultrasound measurement

We performed ultrasound measurements using a pulse-echo phase-sensitive detection technique [44, 45, 65]. Overtone polished 41° X-cut LiNbO_3 resonance transducers are bonded with Thiokol LP-32 to the FIB-prepared parallel sample surfaces. We performed the ultrasound experiments at a frequency of about 30 MHz. We chose the propagation direction $k \parallel b$ with polarization $u \parallel a$, corresponding to the elastic mode $(c_{11} - c_{12})/2$ in the hexagonal lattice [Fig. 1(b)]. The sound velocity, v , is related to the concomitant elastic constant $c_{ij} = \rho v^2$, where ρ is the mass density of the material. The sound velocity is obtained from the time delay of the acoustic signal in the sample.

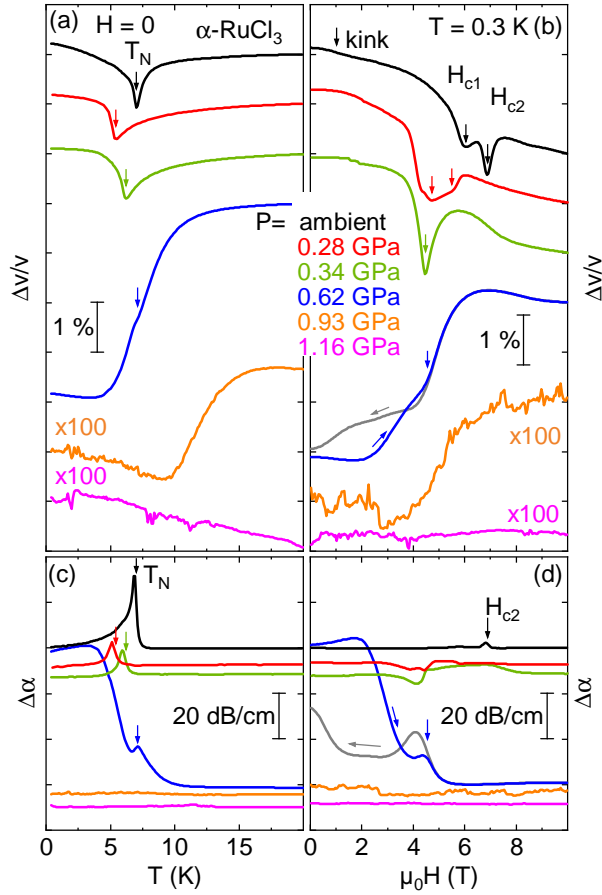


FIG. 2. (a), (b) Relative change of the sound velocity and (c), (d) attenuation of the transverse acoustic mode $(c_{11} - c_{12})/2$ ($k \parallel b$, $u \parallel a$) versus temperature at $H = 0$ (a), (c) and versus magnetic field ($H \parallel a$) at 0.3 K (b), (d), measured at selected hydrostatic pressure values in α -RuCl₃. The arrows indicate the critical temperatures and magnetic fields. The curves are arbitrarily shifted along the y axis for clarity. Relative changes in v and α are depicted by the corresponding scaling bar. Note, that the data at 0.93 and 1.16 GPa in panels (a) and (b) are scaled by a factor of 100.

C. Pressure cell

We used a commercially available cylinder-piston cell from C&T Factory, model CTF-HHPC40 with Daphne 7373 as the pressure medium [66], adapted for ultrasound experiments following the method described in Refs. [67, 68]. The pressure cell was thermally linked to the ³He pot of a commercial ³He cryostat via a copper rod. We attached a calibrated RuO₂ temperature sensor to the pressure cell. The ultrasound experiments in applied magnetic field are performed under zero-field-cooled (ZFC) conditions. For preparing the ultrasound measurement under pressure, we fixed the crystal on a sapphire platform, which is attached to the outer conductor of the coaxial cable in the pressure cell. Up to the highest pressure of 1.16 GPa, we observe multiple ultrasound echoes due to multiple propagation and signal reflections in the sample.

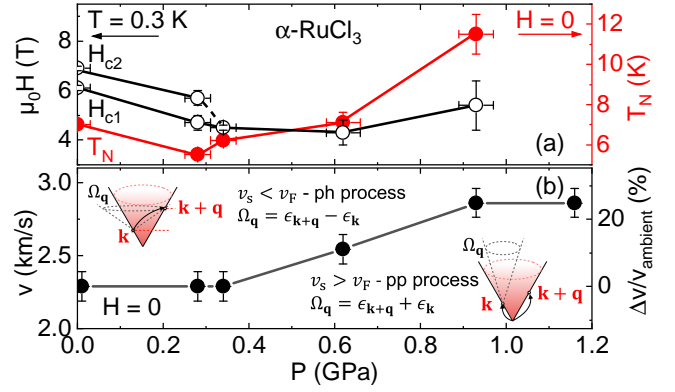


FIG. 3. (a) Pressure dependence of the critical temperature T_N (red solid circles, right scale) in zero magnetic field and critical magnetic fields H_{c1} and H_{c2} (black open circles, left scale) for $H \parallel a$ at 0.3 K in α -RuCl₃. (b) Pressure dependence of the measured sound velocity v of the $(c_{11} - c_{12})/2$ acoustic mode and relative change $[v(P) - v_{\text{ambient}}]/v_{\text{ambient}}$. Insets in (b) show two different phonon scattering processes by Majorana fermions (see text for details).

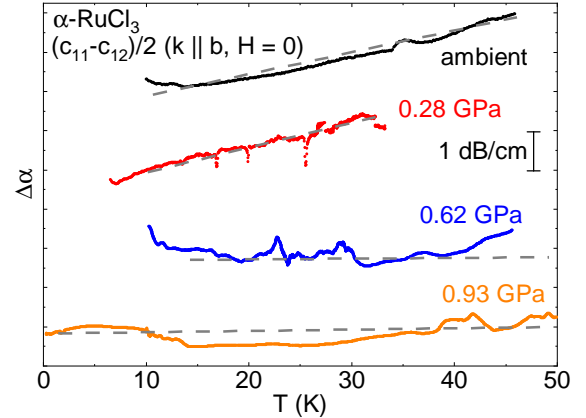


FIG. 4. The attenuation of the transverse acoustic mode $(c_{11} - c_{12})/2$ ($k \parallel b$, $u \parallel a$) versus temperature in α -RuCl₃ at some selected values of the hydrostatic pressure in zero magnetic field beyond the ordered magnetic state. The curves are arbitrarily shifted along the y axis for clarity. The ambient-pressure curve is taken from Ref. [45]. The gray dashed lines are guides to the eye. The low-temperature data were removed close to and below T_N to mask the dominant attenuation anomaly at T_N [45].

Nevertheless, because of the irregular shape of the sample, we focus on the 0th echo (a single sound transmission through the sample) to avoid a superposition with the delayed signals reflected from the sample sides. The pressure is defined from the pressure-dependent superconducting transition in tin [69]. We changed the pressure at room temperature. With slowly cooling the cell to cryogenic temperatures, the hydrostatic conditions remain valid down to 0.3 K, even though a crystallization of daphne 7373 occurs [70].

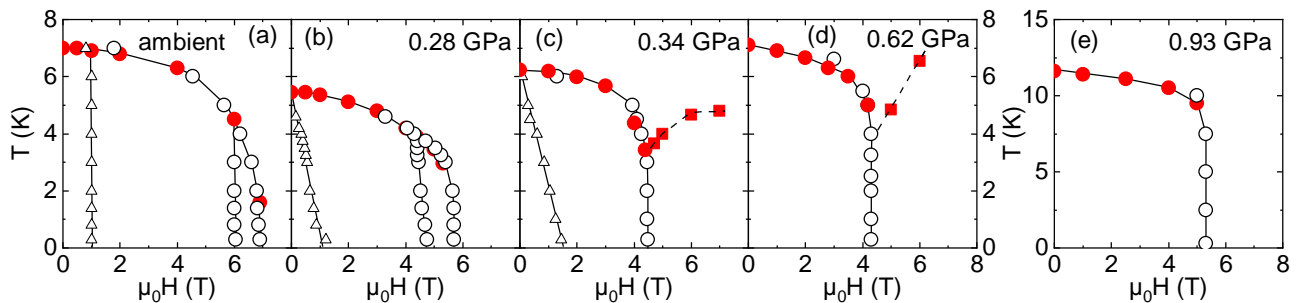


FIG. 5. (a) - (e) H - T phase diagrams ($H \parallel a$) of α - RuCl_3 at various hydrostatic pressures. We extracted critical temperatures from temperature dependent measurements (red circles) and critical fields from field-dependent measurements (open circles and triangles) from our ultrasound results shown in Figs. 2(a) and 2(b). No transitions have been observed at 1.16 GPa. See text for details.

III. RESULTS AND DISCUSSION

B. Ultrasound attenuation

A. Change of the sound velocity under hydrostatic pressure

Figure 2 shows the temperature and magnetic-field dependence of the relative sound velocity change, $\Delta v/v$, for the transverse acoustic mode $(c_{11} - c_{12})/2$ measured at various hydrostatic pressures. At ambient pressure, this mode exhibits pronounced softening, near the AFM ordering temperature, T_N [Fig. 2(a)]. Similar anomalies are observed at magnetic transitions in applied magnetic field, specifically at the critical fields H_{c1} and H_{c2} [Fig. 2(b)] [45]. Much smaller kink-like anomalies are detected in the sound velocity below 2 T, where a magnetic domain rearrangement occurs [45, 71].

As pressure increases, the anomalies in $\Delta v/v$ are significantly modified and their position changes. Specifically, at 0.62 GPa, the sound velocity exhibits a pronounced increase both versus temperature and magnetic field, contrasting with the minima observed at lower pressures. Additionally, the anomaly becomes broader, with the increase in relative velocity occurring over a wider temperature range. At this pressure, the sound velocity increases significantly ($\approx 4\%$) and is accompanied by a strong hysteresis in the field dependence below 4 T, suggesting the presence of a metastable magnetic state. In this state, the dimerized and the non-dimerized phases can coexist, consistent with the strongly first-order nature of the dimerization transition. At 0.93 GPa, only a small, broad step-like anomaly is observed in both the temperature and magnetic-field dependences of the sound velocity [Figs. 2(a) and 2(b)].

Anomalies in the temperature and magnetic-field dependence of the sound velocity, signaling phase transitions, are indicated with arrows in Fig. 2. Accordingly, T_N , H_{c2} , and H_{c1} are plotted as a function of pressure in Fig. 3(a). First, T_N shows a slight decrease with increasing pressure but rises at higher pressures, ultimately surpassing its ambient-pressure value. These trends in T_N are consistent with results reported in Ref. [50]. Remarkably, the absolute value of the sound velocity increases significantly between 0.34 and 0.93 GPa [Fig. 3(b)] indicating a notable stiffening of the $(c_{11} - c_{12})/2$ elastic mode in this pressure range [72].

We now consider the effects of hydrostatic pressure on the sound attenuation in α - RuCl_3 . Figures 2(c) and 2(d) show the sound attenuation at selected pressure values versus temperature and magnetic field, respectively. The sound attenuation exhibits pronounced anomalies at the phase transitions. There is an attenuation maximum at T_N , H_{c2} , and H_{c1} at low pressure values, which transforms in more sophisticated features with pressure increase. The position of the attenuation anomalies matches well with the sound-velocity anomalies. Consistent with the sound-velocity observations, the sound attenuation undergoes a significant change at 0.62 GPa.

Figure 4 shows in enlarged scale the temperature dependence of the sound attenuation of $(c_{11} - c_{12})/2$ at pressure values 0, 0.28, 0.62, and 0.93 GPa in zero magnetic field. To highlight the subtle linear temperature dependence discussed later, we have masked, for clarity, the data points corresponding to the large anomalies associated with the transition into the magnetically ordered state [Figs. 2(c) and 2(d)].

At ambient pressure, the attenuation exhibits a linear temperature dependence with a non-zero slope. This is consistent with the notion that the sound attenuation has contributions from microscopic processes, where a phonon scatters a positive-energy fermionic excitation of the nearby QSL to a higher-energy fermion state, dubbed particle-hole channel [33, 34, 45]. This scattering mechanism is dominant when the sound velocity is smaller than the characteristic Fermi velocity v_F of the fractionalized excitations (discussed further in Sec. IV). As the pressure increases, the slope of the linear temperature dependence decreases. At 0.62 GPa, and discarding noise in the data, the sound attenuation becomes nearly temperature independent. A similar, almost flat temperature profile of the sound attenuation is observed at 0.93 GPa.

In Sec. IV, as a main point of this work, we rationalize this change of slope of the attenuation to arise from a crossover of the scattering of phonons from particle-hole- to particle-particle-like processes in the proximate QSL [33, 34, 45]. On the one hand, this is consistent with the experimentally observed increase of the sound velocity [see Fig. 3(b)]. On the other hand, pressure also modifies the effective magnetic exchange couplings. This can further promote a change of

the scattering mechanism. Both, first-principles calculations [54, 73] and quantum-chemistry analyses [74] have highlighted a significant dependence of magnetic coupling constants on pressure. The various magnetic interactions in α -RuCl₃ respond very differently to lattice variations, with the Kitaev interaction being the most sensitive. We examine these trends in detail in Sec. IV. We will show, that not only the variation of the sound velocity, but also of the Majorana-fermion velocity is a key parameter for the sound attenuation in α -RuCl₃ under pressure.

C. Pressure dependent H - T phase diagram

Using the positions of the acoustic anomalies related to the phase transitions (Fig. 2), we construct the H - T phase diagrams of α -RuCl₃ for selected pressures, as shown in Fig. 5.

The H - T phase diagram at ambient pressure shown in Fig. 5(a) agrees with the H - T phase diagram we reported in Ref. [45], except that the crossover regime beyond the ordered state related to the spin-gap above H_{c2} , detected by the acoustic mode c_{11} [45], is not observed in $(c_{11} - c_{12})/2$ reported here. As pressure increases, the H - T phase diagram undergoes significant modifications. The low-field anomaly near 1 T, related to domain rearrangements in magnetic field [71], is suppressed at 0.62 GPa. Additionally, the transition at H_{c1} indicating a change in the magnetic structure between zigzag phases with different stacking orders [11, 38, 75] is not detected above 0.28 GPa, suggesting that H_{c1} and H_{c2} may merge around 0.3 GPa. The anomalies marked by red squares at 0.34 and 0.62 GPa might be related to remnants of phases with different stacking orders, although this interpretation remains uncertain. Above 0.93 GPa, no evidence of 3D magnetic order is detected.

These findings highlight that pressure significantly alters the magnetic landscape, suppressing specific transitions, merging critical fields, and eliminating 3D magnetic order. In turn, the response to pressure reveals an intricate interplay between stacking order, spin gaps, and magnetic transitions.

IV. DISCUSSION

As we discussed previously [45], the temperature and in-plane magnetic-field dependence of the sound attenuation in α -RuCl₃ is consistent with theoretical predictions that phonons are scattered by fractionalized excitations arising from the proximity of α -RuCl₃ to a Kitaev QSL [33, 34, 46–49]. We showed [45], that the sound attenuation is linear in temperature when the phonon velocity v_s is smaller than the characteristic velocity of the low-energy fermionic excitations, v_F , as observed for the transverse phonon mode, $(c_{11} - c_{12})/2$. Moreover, the attenuation is almost temperature independent with a slight downturn in the case of longitudinal mode c_{11} , which is consistent with a sound velocity slightly exceeding v_F . These different temperature dependences of the sound attenuation of the longitudinal and transverse phonon mode arise from the underlying scattering

mechanisms. For $v_s < v_F$, a phonon excites an occupied fermion state to a higher-energy state [particle-hole (ph) channel]. In contrast, for $v_s > v_F$, the dominant process involves the phonon decaying into two fermions, both with positive energy [particle-particle (pp) channel] [33, 34].

Here, we start by investigating the temperature dependence of the sound attenuation in the pure Kitaev model, incorporating a pressure-dependent variation of the Kitaev interaction as proposed in Ref. [54]. This study demonstrates that the Kitaev interaction is highly sensitive to applied pressure. At ambient pressure, it is the dominant interaction in the system and it is ferromagnetic in nature. However, as pressure increases, the Kitaev interaction acquires a strong positive contribution, eventually leading to a sign change at sufficiently high pressures. Within the pressure range considered in this study (up to approximately 1 GPa), the dominant effect of pressure is a reduction in the magnitude of the Kitaev interaction.

Our results for the pure Kitaev model are presented in Figs. 6(a) - 6(c). In panel (a), the spectrum of fermionic excitations for the Kitaev model is shown, computed with $K = -7$ meV at ambient pressure. The characteristic dispersing modes, arising from free Majoranas hopping on the lattice, feature the Dirac cones at the K points of the Brillouin zone. Additionally, the flat bands correspond to the static Z_2 fluxes. Panels (b) and (c) present the computed Fermi velocity and sound attenuation, respectively, for varying values of the Kitaev interaction. Based on the trend reported in Ref. [54], the Kitaev interaction values K are taken to be -7, -5.25, -3, and -1.75 meV for the four pressure values $P_0 = 0$, $P_1 = 0.28$ GPa, $P_2 = 0.62$ GPa, and $P_3 = 0.93$, respectively.

In Fig. 6(b), the Fermi velocity v_F is compared with the experimental sound velocity shown in Fig. 3(b). We estimate v_F from the slope of the Dirac cones. At ambient pressure, $v_F \simeq 2746$ m/s (18 meV Å), consistent with previous estimates [76]. With increasing pressure, v_F decreases and, just above 0.2 GPa, becomes smaller than the sound velocity. This marks a change in the phonon-attenuation mechanism, shifting from ph-scattering to pp-scattering. This change is evident in the sound-attenuation behavior shown in Fig. 6(c). We see a monotonically increasing attenuation at P_0 , which arises from pure ph-scattering of the acoustic phonons in the regime $v_s < v_F$. At P_1 , v_s is already slightly larger than v_F , placing the system in the pp-scattering regime, where attenuation decreases with temperature as low-energy states become occupied. However, we observe at $P_1 = 0.28$ GPa an increase in attenuation for temperatures above 10 K (Fig. 4). This arises due to ph-scattering, which becomes significant as higher-energy states start to populate. Although we estimate $v_s > v_F$, the difference between the two velocities is very small, allowing a ph-contribution from higher-energy states away from the fermionic cone. At P_2 and P_3 , the system is well within the pp-scattering regime.

The experimentally observed change in the temperature dependence of the sound attenuation occurs at slightly higher pressures (see Fig. 4). Using a more suitable ansatz, we compute the sound attenuation within the J - K - Γ model [Figs. 6(d)-6(f)], in which we incorporated the pressure-dependent variation of the coupling constants. Since the generic J - K - Γ

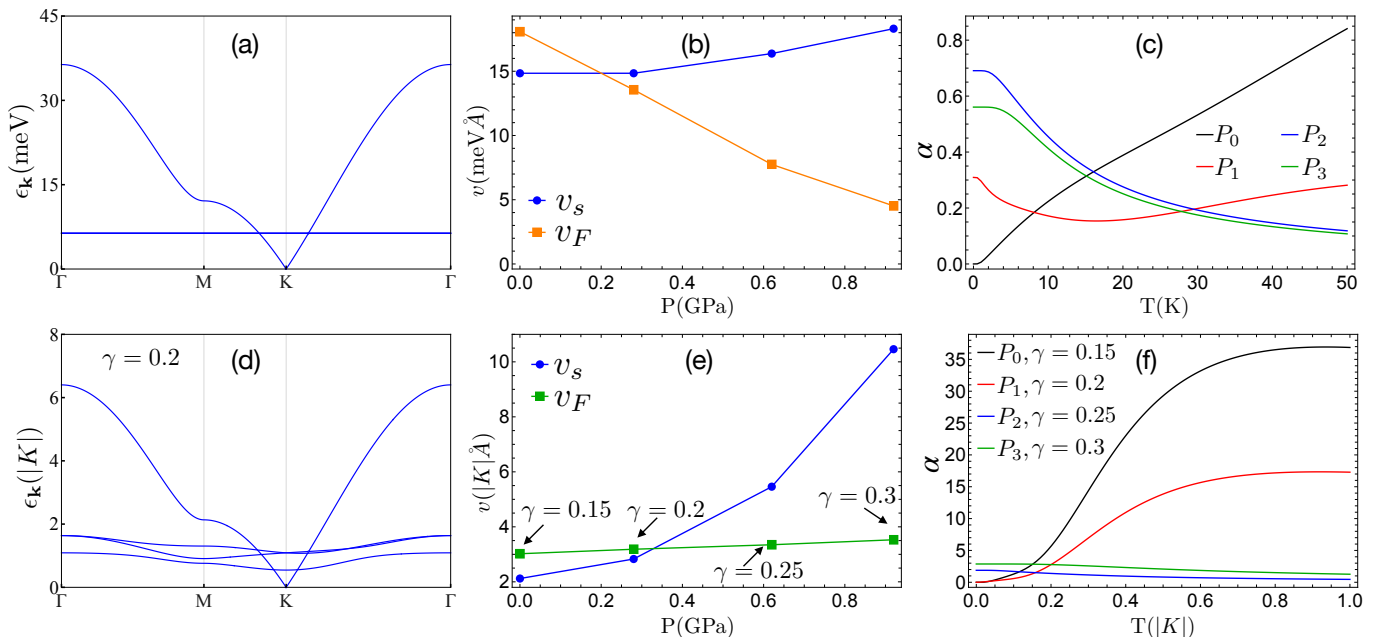


FIG. 6. Spectrum of fermionic excitations for (a) the Kitaev model with $K = -7$ meV and (d) the J - K - Γ model with $\gamma = -J/|K| = \Gamma/|K| = 0.2$. Panels (b) and (e) compare the experimentally measured sound velocity, v_s , with the theoretically estimated Fermi velocity, v_F , for the two models as a function of pressure. Panels (c) and (f) present the computed sound attenuation of the transverse acoustic mode $(c_{11} - c_{12})/2$ versus temperature for various pressures for the pure Kitaev model and the J - K - Γ model, respectively. In (c), the attenuation is due to only ph-processes at P_0 , and only due to pp-processes at P_1 , P_2 , and P_3 . In (f), the attenuation of phonons is dominated by ph-processes at P_0 and P_1 and by pp-processes at P_2 and P_3 . Our calculations follow the pressure dependence of exchange couplings as suggested by ab-initio calculations [54]. In (b) and (c), the pure Kitaev model incorporates the pressure-induced reduction of the Kitaev interaction, scaled to $K = -7$ meV at ambient pressure. In (e) and (f), the J - K - Γ model adopts the pressure-dependent ratio $\gamma = -J/|K| = \Gamma/|K|$ from [54], while ensuring the system remains in the quantum-spin-liquid state (see text for details). In (d)-(f), all quantities (energies, temperatures, velocities) are expressed in units of $|K|$, whereas (a)-(c) use physical units.

model is not exactly solvable, our calculations are performed using a self-consistent slave-fermion mean-field approach, as described in Ref. [47]. The spectrum of the J - K - Γ model with $\gamma = -J/|K| = \Gamma/|K| = 0.2$ is shown in Fig. 6(d). The original dispersing mode is only slightly modified, with the Dirac cones remaining at the K points and the Fermi velocity of the Dirac cones slightly decreasing. However, the flux bands loose their degeneracy and develop a small, yet noticeable dispersion.

We note that while extending the analysis beyond the pure Kitaev model, we still perform our calculations for parameters of the J - K - Γ model, which correspond to the spin-liquid regime. Specifically, we set $\gamma = 0.2$, which provides a more realistic representation of the coupling parameters in α -RuCl₃ under low-pressure conditions compared to the pure Kitaev model. Nonetheless, we emphasize that this choice does not yield a fully quantitative description of α -RuCl₃.

In Figs. 6(e) and 6(f), we use the overall trend for the change of the exchange parameters reported in [54]. According to this trend, the magnitude of the Kitaev interaction K decreases with increasing pressure, while the Heisenberg interaction J and the off-diagonal interaction Γ are enhanced. In Fig. 6(e), the sound velocity v_s and the Fermi velocity v_F are plotted for different values of γ . We assume that γ , representing the relative strengths of the Heisenberg interaction J

and off-diagonal interaction Γ , increases with pressure from P_0 to P_3 . In this case, the sound velocity v_s surpasses the Fermi velocity v_F at a pressure slightly higher, as estimated in the pure Kitaev model.

The resulting sound attenuation is presented in Fig. 6(f). Similar to the pure Kitaev model, the sound attenuation at the lowest two pressures, P_0 and P_1 , exhibits a roughly linear temperature dependence over a certain range of temperatures, followed by saturation and a subsequent decrease at high temperatures (not shown). At higher pressures, P_2 and P_3 , the sound attenuation becomes nearly temperature independent. This behavior can be attributed to the dominant scattering mechanisms: At P_0 and P_1 , the attenuation is primarily governed by ph-processes, whereas at P_2 and P_3 , it is dominated entirely by pp-scattering.

Overall, we obtain that in both, the pure Kitaev and the J - K - Γ models, the sound attenuation changes from a (quasi-) linear increase with temperature to a (weakly) decreasing or almost temperature-independent behavior as pressure is increased. This is similar as observed in experiment, as shown in Fig. 4. We strongly emphasize, that our aim is not to quantitatively describe the variation with pressure of the measured sound attenuation. Instead, and far more important, independent of the model used, we find a pressure-induced crossing, above which the calculated Fermi velocity of the QSL quasi-

particles becomes smaller as the experimentally determined sound velocity. This can favorably explain the observed temperature dependence of the sound attenuation (Fig. 4). Fine details of the temperature and pressure variations of $\Delta\alpha$ are certainly beyond our calculations.

V. SUMMARY

We have presented an ultrasound study of α -RuCl₃ under hydrostatic pressures up to 1.16 GPa. Anomalies in the sound velocity allows us to extract the H - T phase diagrams over a wide range of pressures. At ambient pressure, we identify a marked softening of the acoustic mode $(c_{11} - c_{12})/2$ at T_N , highlighting strong magnetoelastic coupling between lattice vibrations and magnetic degrees of freedom. We find this coupling to persists at temperatures well above the transition into the disordered state [Fig. 2(a)].

The linear temperature dependence of the sound attenuation of $(c_{11} - c_{12})/2$ at ambient pressure beyond the ordered state is consistent with phonons scattered by Majorana fermions in a process dominated by particle-hole excitations. As pressures increases, however, the sound attenuation becomes nearly temperature independent, suggesting a crossover of the scattering channel from a ph-dominated to rather a pp-regime. This crossover can be understood by a reversal of the magnitudes of the sound and Fermi velocities from $v_s < v_F$ at low pressure to $v_s > v_F$ above 0.28 GPa. This reversal is of twofold origin. I.e., from our experimental findings, the measured sound velocity of $(c_{11} - c_{12})/2$ increases substan-

tially with pressure, while from our theoretical analysis, the Fermi velocities of an effective J - K - Γ model remain almost invariant with pressure.

Overall, our findings provide compelling evidence for the tunability of phonon dynamics in α -RuCl₃ through hydrostatic pressure and further improve our understanding of spin-strain interactions in Kitaev magnets.

ACKNOWLEDGMENTS

We gratefully acknowledge our previous collaboration with Mengxing Ye and Peter Stavropoulos and discussions with Roser Valenti, which significantly contributed to shaping our understanding and approach in this work. We acknowledge support of the HLD at HZDR, member of the European Magnetic Field Laboratory (EMFL). Work of S.Z., A.H., W.B., and J.W. has been supported in part by the DFG through SFB 1143 (project-id 247310070). Work of A.H., J.W., and S.Z. has been supported in part by the DFG trough excellence cluster *ct.qmat* (EXC 2147, project-id 39085490). W.B. acknowledges kind hospitality of the PSM, Dresden. The work of N.B.P. and S.S. was supported by the U.S. Department of Energy, Office of Science, Basic Energy Sciences under Award No. DE-SC0018056. N.B.P. also acknowledges the hospitality and partial support of the Technical University of Munich – Institute for Advanced Study. The work of V.T. was supported by the DFG through Transregional Research Collaboration TRR 80 (Augsburg, Munich, and Stuttgart) as well as by the project ANCD 20.80009.5007.19 (Moldova).

-
- [1] G. Jackeli and G. Khaliullin, Mott Insulators in the Strong Spin-Orbit Coupling Limit: From Heisenberg to a Quantum Compass and Kitaev Models, *Phys. Rev. Lett.* **102**, 017205 (2009).
 - [2] H. Takagi, T. Takayama, G. Jackeli, G. Khaliullin, and S. E. Nagler, Concept and realization of Kitaev quantum spin liquids, *Nat. Rev. Phys.* **1**, 264 (2019).
 - [3] S. Trebst and C. Hickey, Kitaev materials, *Phys. Rep.* **950**, 1 (2022).
 - [4] I. Rousochatzakis, N. B. Perkins, Q. Luo, and H.-Y. Kee, Beyond Kitaev physics in strong spin-orbit coupled magnets, *Reports on Progress in Physics* **87**, 026502 (2024).
 - [5] A. Kitaev, Anyons in an exactly solved model and beyond, *Annals of Physics* **321**, 2 (2006), january Special Issue.
 - [6] K. W. Plumb, J. P. Clancy, L. J. Sandilands, V. V. Shankar, Y. F. Hu, K. S. Burch, H.-Y. Kee, and Y.-J. Kim, α -RuCl₃: A Spin-Orbit Assisted Mott Insulator on a Honeycomb Lattice, *Phys. Rev. B* **90**, 041112(R) (2014).
 - [7] J. A. Sears, M. Songvilay, K. W. Plumb, J. P. Clancy, Y. Qiu, Y. Zhao, D. Parshall, and Y.-J. Kim, Magnetic Order in α -RuCl₃: A Honeycomb-Lattice Quantum Magnet with Strong Spin-Orbit Coupling, *Phys. Rev. B* **91**, 144420 (2015).
 - [8] Y. Kasahara, T. Ohnishi, Y. Mizukami, O. Tanaka, S. Ma, K. Sugii, N. Kurita, H. Tanaka, J. Nasu, Y. Motome, T. Shibauchi, and Y. Matsuda, Majorana quantization and half-integer thermal quantum Hall effect in a Kitaev spin liquid, *Nature (London)* **559**, 227 (2018).
 - [9] O. Tanaka, Y. Mizukami, R. Harasawa, K. Hashimoto, K. Hwang, N. Kurita, H. Tanaka, S. Fujimoto, Y. Matsuda, E.-G. Moon, and T. Shibauchi, Thermodynamic evidence for a field-angle-dependent Majorana gap in a Kitaev spin liquid, *Nat. Phys.* **18**, 429 (2022).
 - [10] T. Yokoi, S. Ma, Y. Kasahara, S. Kasahara, T. Shibauchi, N. Kurita, H. Tanaka, J. Nasu, Y. Motome, C. Hickey, S. Trebst, and Y. Matsuda, Half-integer quantized anomalous thermal Hall effect in the Kitaev material candidate α -RuCl₃, *Science* **373**, 568 (2021).
 - [11] C. Balz, L. Janssen, P. Lampen-Kelley, A. Banerjee, Y. H. Liu, J.-Q. Yan, D. G. Mandrus, M. Vojta, and S. E. Nagler, Field-induced intermediate ordered phase and anisotropic interlayer interactions in α -RuCl₃, *Phys. Rev. B* **103**, 174417 (2021).
 - [12] H. Suzuki, H. Liu, J. Bertinshaw, K. Ueda, H. Kim, S. Laha, D. Weber, Z. Yang, L. Wang, H. Takahashi, K. Fürsich, M. Minola, B. V. Lotsch, B. J. Kim, H. Yavaş, M. Daghofer, J. Chaloupka, G. Khaliullin, H. Gretarsson, and B. Keimer, Proximate ferromagnetic state in the Kitaev model material α -RuCl₃, *Nat. Commun.* **12**, 4512 (2021).
 - [13] J. Wagner, A. Sahasrabudhe, R. B. Versteeg, L. Wysocki, Z. Wang, V. Tsurkan, A. Loidl, D. I. Khomskii, H. Hedayat, and P. H. M. van Loosdrecht, Magneto-optical study of metamagnetic transitions in the antiferromagnetic phase of α -RuCl₃, *npj Quantum Mater.* **7**, 28 (2022).
 - [14] S. Bachus, D. A. Kaib, Y. Tokiwa, A. Jesche, V. Tsurkan, A. Loidl, S. Winter, A. Tsirlin, R. Valentí, and P. Gegenwart, Thermodynamic Perspective on Field-Induced Behavior of α -

- RuCl₃, *Phys. Rev. Lett.* **125**, 097203 (2020).
- [15] A. Banerjee, J. Yan, J. Knolle, C. A. Bridges, M. B. Stone, M. D. Lumsden, D. G. Mandrus, D. A. Tennant, R. Moessner, and S. E. Nagler, Neutron scattering in the proximate quantum spin liquid α -RuCl₃, *Science* **356**, 1055 (2017).
- [16] A. U. B. Wolter and C. Hess, Spin liquid evidence at the edge and in bulk, *Nat. Phys.* **18**, 378 (2022).
- [17] J. Knolle, D. L. Kovrizhin, J. T. Chalker, and R. Moessner, Dynamics of a Two-Dimensional Quantum Spin Liquid: Signatures of Emergent Majorana Fermions and Fluxes, *Phys. Rev. Lett.* **112**, 207203 (2014).
- [18] J. Knolle, G.-W. Chern, D. L. Kovrizhin, R. Moessner, and N. B. Perkins, Raman scattering signatures of kitaev spin liquids in A₂IrO₃ iridates with $a = \text{Na}$ or Li , *Phys. Rev. Lett.* **113**, 187201 (2014).
- [19] B. Perreault, J. Knolle, N. B. Perkins, and F. J. Burnell, Theory of raman response in three-dimensional kitaev spin liquids: Application to β - and γ -Li₂IrO₃ compounds, *Phys. Rev. B* **92**, 094439 (2015).
- [20] B. Perreault, J. Knolle, N. B. Perkins, and F. J. Burnell, Resonant raman scattering theory for kitaev models and their majorana fermion boundary modes, *Phys. Rev. B* **94**, 104427 (2016).
- [21] I. Rousochatzakis, S. Kourtis, J. Knolle, R. Moessner, and N. B. Perkins, Quantum spin liquid at finite temperature: Proximate dynamics and persistent typicality, *Phys. Rev. B* **100**, 045117 (2019).
- [22] G. B. Halász, N. B. Perkins, and J. van den Brink, Resonant Inelastic X-Ray Scattering Response of the Kitaev Honeycomb Model, *Phys. Rev. Lett.* **117**, 127203 (2016).
- [23] G. B. Halász, S. Kourtis, J. Knolle, and N. B. Perkins, Observing spin fractionalization in the kitaev spin liquid via temperature evolution of indirect resonant inelastic x-ray scattering, *Phys. Rev. B* **99**, 184417 (2019).
- [24] Y. Wan and N. P. Armitage, Resolving continua of fractional excitations by spinon echo in the 2d coherent spectroscopy, *Phys. Rev. Lett.* **122**, 257401 (2019).
- [25] R. G. Pereira and R. Egger, Electrical access to ising anyons in kitaev spin liquids, *Phys. Rev. Lett.* **125**, 227202 (2020).
- [26] M. Udagawa, S. Takayoshi, and T. Oka, Scanning tunneling microscopy as a single majorana detector of kitaev's chiral spin liquid, *Phys. Rev. Lett.* **126**, 127201 (2021).
- [27] A. P. Joy and A. Rosch, Dynamics of visons and thermal hall effect in perturbed kitaev models, *Phys. Rev. X* **12**, 041004 (2022).
- [28] T. Bauer, L. R. D. Freitas, R. G. Pereira, and R. Egger, Scanning tunneling spectroscopy of majorana zero modes in a kitaev spin liquid, *Phys. Rev. B* **107**, 054432 (2023).
- [29] W.-H. Kao, G. B. Halász, and N. B. Perkins, Dynamics of vacancy-induced modes in the non-abelian kitaev spin liquid, *Phys. Rev. B* **109**, 125150 (2024).
- [30] W.-H. Kao, N. B. Perkins, and G. B. Halász, Vacancy spectroscopy of non-abelian kitaev spin liquids, *Phys. Rev. Lett.* **132**, 136503 (2024).
- [31] Y. Vinkler-Aviv and A. Rosch, Approximately Quantized Thermal Hall Effect of Chiral Liquids Coupled to Phonons, *Phys. Rev. X* **8**, 031032 (2018).
- [32] M. Ye, G. B. Halász, L. Savary, and L. Balents, Quantization of the Thermal Hall Conductivity at Small Hall Angles, *Phys. Rev. Lett.* **121**, 147201 (2018).
- [33] A. Metavitsiadis and W. Brenig, Phonon renormalization in the kitaev quantum spin liquid, *Phys. Rev. B* **101**, 035103 (2020).
- [34] M. Ye, R. M. Fernandes, and N. B. Perkins, Phonon dynamics in the kitaev spin liquid, *Phys. Rev. Research* **2**, 033180 (2020).
- [35] H. Li, T. T. Zhang, A. Said, G. Fabbris, D. G. Mazzone, J. Q. Yan, D. Mandrus, G. B. Halász, S. Okamoto, S. Murakami, M. P. M. Dean, H. N. Lee, and H. Miao, Giant phonon anomalies in the proximate Kitaev quantum spin liquid α -RuCl₃, *Nat. Commun.* **12**, 3513 (2021).
- [36] V. Kocsis, D. A. S. Kaib, K. Riedl, S. Gass, P. Lampen-Kelley, D. G. Mandrus, S. E. Nagler, N. Pérez, K. Nielsch, B. Büchner, A. U. B. Wolter, and R. Valentí, Magnetoelastic coupling anisotropy in the kitaev material α -RuCl₃, *Phys. Rev. B* **105**, 094410 (2022).
- [37] D. A. S. Kaib, S. Biswas, K. Riedl, S. M. Winter, and R. Valentí, Magnetoelastic coupling and effects of uniaxial strain in α -RuCl₃ from first principles, *Phys. Rev. B* **103**, L140402 (2021).
- [38] R. Schönemann, S. Imajo, F. Weickert, J. Yan, D. G. Mandrus, Y. Takano, E. L. Brosha, P. F. S. Rosa, S. E. Nagler, K. Kindo, and M. Jaime, Thermal and magnetoelastic properties of α -RuCl₃ in the field-induced low-temperature states, *Phys. Rev. B* **102**, 214432 (2020).
- [39] R. Hentrich, A. U. B. Wolter, X. Zotos, W. Brenig, D. Nowak, A. Isaeva, T. Doert, A. Banerjee, P. Lampen-Kelley, D. G. Mandrus, S. E. Nagler, J. Sears, Y.-J. Kim, B. Büchner, and C. Hess, Unusual phonon heat transport in α -RuCl₃: Strong spin-phonon scattering and field-induced spin gap, *Phys. Rev. Lett.* **120**, 117204 (2018).
- [40] S. Reschke, V. Tsurkan, S.-H. Do, K.-Y. Choi, P. Lunkenheimer, Z. Wang, and A. Loidl, Terahertz excitations in α -RuCl₃: Majorana fermions and rigid-plane shear and compression modes, *Phys. Rev. B* **100**, 100403 (2019).
- [41] J. A. N. Bruin, R. R. Claus, Y. Matsumoto, N. Kurita, H. Tanaka, and H. Takagi, Robustness of the thermal Hall effect close to half-quantization in α -RuCl₃, *Nat. Phys.* **18**, 401–402 (2022).
- [42] M. Yamashita, J. Gouchi, Y. Uwatoko, N. Kurita, and H. Tanaka, Sample dependence of half-integer quantized thermal hall effect in the kitaev spin-liquid candidate α -RuCl₃, *Phys. Rev. B* **102**, 220404 (2020).
- [43] R. Truell, C. Elbaum, and B. B. Chick, *Ultrasonic Methods in Solid State Physics* (Academic Press, Inc., New York, 1969).
- [44] B. Lüthi, *Physical Acoustics in the Solid State* (Springer-Verlag, Berlin Heidelberg, New York, 2005).
- [45] A. Hauspurg, S. Zherlitsyn, T. Helm, V. Felea, J. Wosnitza, V. Tsurkan, K.-Y. Choi, S.-H. Do, M. Ye, W. Brenig, and N. B. Perkins, Fractionalized excitations probed by ultrasound, *Phys. Rev. B* **109**, 144415 (2024).
- [46] K. Feng, M. Ye, and N. B. Perkins, Temperature evolution of the phonon dynamics in the kitaev spin liquid, *Phys. Rev. B* **103**, 214416 (2021).
- [47] S. Singh, P. P. Stavropoulos, and N. B. Perkins, Phonon dynamics in the generalized kitaev spin liquid, *Phys. Rev. B* **107**, 214428 (2023).
- [48] S. Singh, P. P. Stavropoulos, and N. B. Perkins, Phonon dynamics in the chiral kitaev spin liquid, *Phys. Rev. B* **110**, 094431 (2024).
- [49] V. Dantas, W.-H. Kao, and N. B. Perkins, Phonon dynamics in the site-disordered kitaev spin liquid, *Phys. Rev. B* **110**, 104425 (2024).
- [50] Y. Cui, J. Zheng, K. Ran, J. Wen, Z.-X. Liu, B. Liu, W. Guo, and W. Yu, High-pressure magnetization and nmr studies of α -RuCl₃, *Phys. Rev. B* **96**, 205147 (2017).
- [51] T. Biesner, S. Biswas, W. Li, Y. Saito, A. Pustogow, M. Altmeyer, A. U. B. Wolter, B. Büchner, M. Roslova, T. Doert, S. M. Winter, R. Valentí, and M. Dressel, Detuning the honeycomb of α -RuCl₃: Pressure-dependent optical studies reveal broken symmetry, *Phys. Rev. B* **97**, 220401 (2018).

- [52] G. Bastien, G. Garbarino, R. Yadav, F. J. Martinez-Casado, R. Beltrán Rodríguez, Q. Stahl, M. Kusch, S. P. Limandri, R. Ray, P. Lampen-Kelley, D. G. Mandrus, S. E. Nagler, M. Roslova, A. Isaeva, T. Doert, L. Hozoi, A. U. B. Wolter, B. Büchner, J. Geck, and J. van den Brink, Pressure-induced dimerization and valence bond crystal formation in the kitaev-heisenberg magnet α - RuCl_3 , *Phys. Rev. B* **97**, 241108 (2018).
- [53] X. Wang, F. Zhu, N. Qureshi, K. Beauvois, J. Song, T. Mueller, T. Brückel, and Y. Su, Hydrostatic pressure effects in the kitaev quantum magnet α - RuCl_3 : A single-crystal neutron diffraction study, arXiv:2304.00632 (2023).
- [54] B. Wolf, D. A. S. Kaib, A. Razpopov, S. Biswas, K. Riedl, S. M. Winter, R. Valentí, Y. Saito, S. Hartmann, E. Vinokurova, T. Doert, A. Isaeva, G. Bastien, A. U. B. Wolter, B. Büchner, and M. Lang, Combined experimental and theoretical study of hydrostatic he-gas pressure effects in α - RuCl_3 , *Phys. Rev. B* **106**, 134432 (2022).
- [55] Q. Stahl, T. Ritschel, G. Gararino, F. Cova, A. Isaeva, T. Doert, and J. Geck, Pressure-tuning of α - RuCl_3 towards a quantum spin liquid, *Nat. Commun.* **15**, 8142 (2024).
- [56] W. B. Daniels and M. G. Ryschkewitsch, Simple double diaphragm press for diamond anvil cells at low temperatures, *Rev. Sci. Instrum.* **54**, 115 (1983).
- [57] Z. Wang, J. Guo, F. F. Tafti, A. Hegg, S. Sen, V. A. Sidorov, L. Wang, S. Cai, W. Yi, Y. Zhou, H. Wang, S. Zhang, K. Yang, A. Li, X. Li, Y. Li, J. Liu, Y. Shi, W. Ku, Q. Wu, R. J. Cava, and L. Sun, Pressure-induced melting of magnetic order and emergence of a new quantum state in α - RuCl_3 , *Phys. Rev. B* **97**, 245149 (2018).
- [58] K. Momma and F. Izumi, VESTA3 for three-dimensional visualization of crystal, volumetric and morphology data, *J. Appl. Crystallogr.* **44**, 1272 (2011).
- [59] S. Reschke, F. Mayr, S. Widmann, H.-A. K. von Nidda, V. Tsurkan, M. V. Eremin, S.-H. Do, K.-Y. Choi, Z. Wang, and A. Loidl, Sub-gap optical response in the Kitaev spin-liquid candidate α - RuCl_3 , *J. Phys.: Condens. Matter* **30**, 475604 (2018).
- [60] X. Mi, X. Wang, H. Gui, M. Pi, T. Zheng, K. Yang, Y. Gan, P. Wang, A. Li, A. Wang, L. Zhang, Y. Su, Y. Chai, and M. He, Stacking faults in α - RuCl_3 revealed by local electric polarization, *Phys. Rev. B* **103**, 174413 (2021).
- [61] H. B. Cao, A. Banerjee, J.-Q. Yan, C. A. Bridges, M. D. Lumsden, D. G. Mandrus, D. A. Tennant, B. C. Chakoumakos, and S. E. Nagler, Low-temperature crystal and magnetic structure of α - RuCl_3 , *Phys. Rev. B* **93**, 134423 (2016).
- [62] S. Mu, K. D. Dixit, X. Wang, D. L. Abernathy, H. Cao, S. E. Nagler, J. Yan, P. Lampen-Kelley, D. Mandrus, C. A. Polanco, L. Liang, G. B. Halász, Y. Cheng, A. Banerjee, and T. Berlijn, Role of the third dimension in searching for Majorana fermions in α - RuCl_3 via phonons, *Phys. Rev. Research* **4**, 013067 (2022).
- [63] B. W. Lebert, S. Kim, D. A. Prishchenko, A. A. Tsirlin, A. H. Said, A. Alatas, and Y.-J. Kim, Acoustic phonon dispersion of α - RuCl_3 , *Phys. Rev. B* **106**, L041102 (2022).
- [64] I. Yamauchi, M. Hiraishi, H. Okabe, S. Takeshita, A. Koda, K. M. Kojima, R. Kadono, and H. Tanaka, Local spin structure of the α - RuCl_3 honeycomb-lattice magnet observed via muon spin rotation/relaxation, *Phys. Rev. B* **97**, 134410 (2018).
- [65] B. Wolf, B. Lüthi, S. Schmidt, H. Schwenk, M. Sieling, S. Zherlitsyn, and I. Kouroudis, New experimental techniques for pulsed magnetic fields – ESR and ultrasonics, *Physica B: Condensed Matter* **294-295**, 612 (2001).
- [66] D. Staško, J. Prchal, M. Klicpera, S. Aoki, and K. Murata, Pressure media for high pressure experiments, Daphne Oil 7000 series, *High Pressure Research* **40**, 525 (2020).
- [67] S. Mombetsu, T. Murazumi, H. Hidaka, T. Yanagisawa, H. Amitsuka, P.-C. Ho, and M. B. Maple, Study of localized character of 4 f electrons and ultrasonic dispersions in $\text{SmOs}_4\text{Sb}_{12}$ by high-pressure high-frequency ultrasonic measurements, *Phys. Rev. B* **94**, 085142 (2016).
- [68] M. W. Kepa, C. J. Ridley, K. V. Kamenev, and A. D. Huxley, Piston cylinder cell for high pressure ultrasonic pulse echo measurements, *Rev. Sci. Instr.* **87**, 085103 (2016).
- [69] A. Eiling and J. S. Schilling, Pressure and temperature dependence of electrical resistivity of Pb and Sn from 1-300K and 0-10 GPa-use as continuous resistive pressure monitor accurate over wide temperature range; superconductivity under pressure in Pb, Sn and In, *J. Phys. F: Met. Phys.* **11**, 623 (1981).
- [70] K. M. Yokogawa, H. Yoshino, and S. Aoyama, Solidification of high-pressure medium daphne 7373, *Jpn. J. Appl. Phys.* **46**, 3636 (2007).
- [71] J. A. Sears, Y. Zhao, Z. Xu, J. W. Lynn, and Y.-J. Kim, Phase diagram of α - RuCl_3 in an in-plane magnetic field, *Phys. Rev. B* **95**, 180411 (2017).
- [72] We note that the sample size undergoes a change under applied pressure. At room temperature, we verified that the relative length change within the hexagonal plane remains below 3% ($\Delta l/l_0 < 3\%$) for pressures up to 1 GPa. Based on XRD analysis [52], the sample-size change under pressure may be larger at lower temperatures. Since we do not have precise values, we did not include this correction in our analysis. We acknowledge that the reported sound velocity and its relative change might be slightly overestimated.
- [73] D. A. S. Kaib, S. Biswas, K. Riedl, S. M. Winter, and R. Valentí, Magnetoelastic coupling and effects of uniaxial strain in α - RuCl_3 from first principles, *Phys. Rev. B* **103**, L140402 (2021).
- [74] R. Yadav, S. Rachel, L. Hozoi, J. van den Brink, and G. Jackeli, Strain- and pressure-tuned magnetic interactions in honeycomb kitaev materials, *Phys. Rev. B* **98**, 121107 (2018).
- [75] C. Balz, P. Lampen-Kelley, A. Banerjee, J. Yan, Z. Lu, X. Hu, S. M. Yadav, Y. Takano, Y. Liu, D. A. Tennant, M. D. Lumsden, D. Mandrus, and S. E. Nagler, Finite field regime for a quantum spin liquid in α - RuCl_3 , *Phys. Rev. B* **100**, 060405 (2019).
- [76] H. Li, A. Said, J. Q. Yan, D. M. Mandrus, H. N. Lee, S. Okamoto, G. B. Halász, and H. Miao, Divergence of majorana-phonon scattering in kitaev quantum spin liquid, arXiv:2112.02015 (2021).